






RESEARCH ARTICLE | APRIL 22 2024

# Chemical short-range order enhances fracture toughness of medium entropy alloy CoCrNi

Wu-Rong Jian  ; Shuozhi Xu   ; Dengke Chen  ; Irene J. Beyerlein 

 Check for updates

*Appl. Phys. Lett.* 124, 171903 (2024)

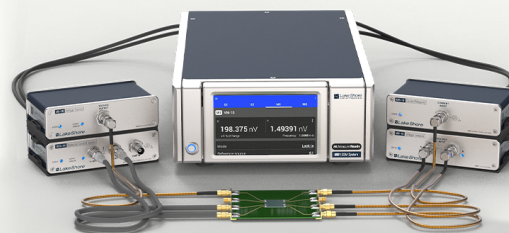
<https://doi.org/10.1063/5.0206532>



## An innovative I-V characterization system for next-gen semiconductor R&D

Unique combination of ultra-low noise sourcing + high-sensitivity lock-in measuring capabilities

[Learn more](#)



# Chemical short-range order enhances fracture toughness of medium entropy alloy CoCrNi

Cite as: Appl. Phys. Lett. **124**, 171903 (2024); doi: [10.1063/5.0206532](https://doi.org/10.1063/5.0206532)

Submitted: 2 March 2024 · Accepted: 8 April 2024 ·

Published Online: 22 April 2024



View Online



Export Citation



CrossMark

Wu-Rong Jian,<sup>1</sup>  Shuozhi Xu,<sup>2,a)</sup>  Dengke Chen,<sup>3</sup>  and Irene J. Beyerlein<sup>4,5</sup> 

## AFFILIATIONS

<sup>1</sup>Department of Mechanical Engineering, Stanford University, Stanford, California 94305, USA

<sup>2</sup>School of Aerospace and Mechanical Engineering, University of Oklahoma, Norman, Oklahoma 73019-1052, USA

<sup>3</sup>Department of Engineering Mechanics, School of Naval Architecture, Ocean and Civil Engineering, Shanghai Jiao Tong University, Shanghai 200240, China

<sup>4</sup>Department of Mechanical Engineering, University of California, Santa Barbara, California 93106-5070, USA

<sup>5</sup>Materials Department, University of California, Santa Barbara, California 93106-5050, USA

**Note:** This paper is part of the APL Special Collection on Era of Entropy: Synthesis, Structure, Properties, and Applications of High Entropy Materials.

<sup>a)</sup> Author to whom correspondence should be addressed: [shuozhixu@ou.edu](mailto:shuozhixu@ou.edu)

## ABSTRACT

Using hybrid molecular dynamics and Monte Carlo simulations, we examine the role of lattice distortion (LD) and chemical short-range ordering (CSRO) on the development of defects ahead of a mode I crack in medium entropy alloy CoCrNi. We show that CSRO noticeably increases fracture toughness. The result can be explained by the effect of CSRO on lowering LD and increasing intrinsic stacking fault energy and the direct impact CSRO has on the energetic barriers for emitting partial dislocations and forming nanotwins from CoCr clusters on the crack tip. CSRO allows the nanotwin domains to further support inelastic deformation, such as dislocation glide and amorphization, leading to stable crack-tip plasticity and postponement of softening. These findings imply that the superior fracture toughness in CoCrNi can be attributed to the non-negligible CSRO that naturally exists.

Published under an exclusive license by AIP Publishing. <https://doi.org/10.1063/5.0206532>

Owing to many superior mechanical properties, such as high creep resistance<sup>1</sup> and excellent ductility,<sup>2</sup> multi-principal element alloys (MPEAs), including high entropy alloys and medium entropy alloys (MEAs), have attracted worldwide attention.<sup>3–6</sup> As a premier example, the CoCrNi MEA has demonstrated an outstanding combination of high strength and fracture toughness at ultra-low and room temperatures.<sup>7–9</sup>

MPEAs contain at least three principal elements in similar proportions and consequently bear an unusual chemical inhomogeneity with element types randomly varying from one lattice site to another. The deviation from traditional alloys leads to severe lattice distortion (LD) and randomly varying strengths in bonds between neighboring atoms.<sup>10,11</sup> While many MPEAs consist of different elements that are randomly distributed, in some MPEAs, chemical short-range ordering (CSRO), the thermodynamic preference for certain elements to pair or cluster, can be significant, as demonstrated through experimental studies on CoCrNi.<sup>12–14</sup>

Many studies have used atomistic simulations to identify the influence of LD and CSRO on the properties of CoCrNi. Molecular

statics (MS) simulations have revealed non-negligible effects of LD and/or CSRO on lattice parameter, elastic constants,<sup>15</sup> and generalized stacking fault energies (GSFE).<sup>16</sup> Molecular dynamics (MD) simulations of simple tests, such as uniaxial loading and shear loading, have reported increases in strength due to LD and CSRO,<sup>17,18</sup> both of which are shown to be responsible for reducing dislocation mobility<sup>15,19</sup> and promoting nanotwinning.<sup>20,21</sup> MD studies have also exposed CoCrNi's noticeable effects under more complex conditions, such as melting,<sup>22</sup> shock dynamics,<sup>23</sup> nanoindentation,<sup>24</sup> creep,<sup>25</sup> and quasi-isentropic compression.<sup>26</sup> It was found that shock-induced amorphization<sup>27</sup> and phase transitions<sup>26</sup> are promoted by LD and/or CSRO.

Only recently, the deformation mechanisms occurring at the crack-tip have been investigated in MPEAs. Load-induced amorphization at the crack tip, which was observed in CoCrFeMnNi MPEA in experiments and MD simulations, was proposed as a strain energy dissipating mechanism that explained its high toughness.<sup>28,29</sup> Recently, the role of LD on dislocation behavior at the crack tip in the CoCrCuFeNi MPEA was studied using MD simulations.<sup>30</sup> The study found that LD induces local fluctuations in surface energy, which can

lead to crack arrest. It was also revealed that the effect of LD can depend on load orientation. Zhu *et al.*<sup>31</sup> recently examined the role of both LD and CSRO on energy release rates at the crack tip (J-integral) in CoCrNi. They found that CSRO increases the activation energy barrier of partial dislocations, while LD decreases it. The deformation mechanisms ahead of the crack-tip in all situations were dislocation emission and nanotwinning, occurring on a one slip system.

In this work, we seek to further identify and isolate the roles of LD and CSRO on the mechanisms ahead of a mode I crack in CoCrNi. We utilize LAMMPS<sup>32</sup> to perform atomistic simulations, where the embedded-atom method potential developed by Li *et al.*<sup>15</sup> is applied. This potential has been used in a series of atomistic simulations involving mechanical deformation in CoCrNi MEA.<sup>15,16,18,20,26,27,33,34</sup> An A-atom potential, via the method in Ref. 35, is generated to describe a pure metal with the equivalent lattice constants and elastic moduli as the CoCrNi MEA.<sup>20,22,23,26,36</sup> Atomic structures are visualized by the polyhedral template matching (PTM) method<sup>37</sup> implemented in OVITO<sup>38</sup> to distinguish face-centered cubic (FCC), body-centered cubic, and hexagonal close-packed (HCP) structures from one another.

For constructing MEA atomic models, a pure Ni single crystal is built first, whose crystallographic orientations ( $[\bar{1}\bar{1}2]$ ,  $[111]$ , and  $[\bar{1}10]$ ) are aligned, respectively, with the  $x$ -,  $y$ -, and  $z$ -axes. These orientations are common in studies of crack events in FCC metals.<sup>28–31</sup> The  $\{111\}$  plane is the preferred cleavage plane in FCC systems and the normal to the glide planes on which dislocations are emitted would lie within the  $x$ - $y$  plane. Figure 1(e) presents a schematic of the model.  $L_x$ ,  $L_y$ , and  $L_z$  are about 60, 60, and 10 nm, respectively.

Next, the Ni model is used to generate the CoCrNi MEAs with a uniformly random atomic distribution, i.e., random solid solution (RSS), or two prescribed degrees of CSRO. For the former [Fig. 1(b)], we replace the Ni atoms with Co or Cr atoms randomly. For the latter [Figs. 1(c) and 1(d)], the hybrid MD/Monte Carlo (MC) simulation method is used to create CoCrNi MEA structures with CSRO. Through MC calculations under the semi-grand-canonical ensemble

at 1500 K, we determine the chemical potential differences among the three elements:  $\Delta\mu_{\text{Co-Ni}} = -0.021$  and  $\Delta\mu_{\text{Cr-Ni}} = 0.32$  eV. Then, a hybrid MD/MC simulation is carried out at an annealing temperature of 950 or 350 K, starting from the pure Ni samples. In MD simulations, a time step size of 2.5 fs is used, and an NPT ensemble is applied to maintain the temperature (950 or 350 K).<sup>15</sup> For every 20 MD steps, there is one MC cycle, wherein a quarter of the atoms attempt to swap Ni atoms for Co or Cr atoms under the variance-constrained semi-grand-canonical ensemble. The variance constraint parameter is 1000. After 100 000 MC cycles, we achieve equilibrium configurations with the equimolar composition, which is subsequently quenched to 1 K and followed by energy minimization, while all three normal stresses are zero.<sup>39</sup> The resulting samples represent two different degrees of CSRO. As a basis for comparison with the random and CSRO samples mentioned above, an A-atom sample [Fig. 1(a)] is created. In what follows, “A-atom,” “RSS,” “950KCSRO,” and “350KCSRO” denote, respectively, the A-atom sample, the RSS CoCrNi, and the CoCrNi with CSRO resulting from annealing at 950 and 350 K. As shown in Figs. 1(c) and 1(d), the 350KCSRO sample has a higher degree of CSRO than the 950KCSRO one.

As mentioned, comparing across the three MEAs and the A-atom sample is intended to reveal the effects of LD and CSRO on dynamic processes. First, it is worth noting some interactions between LD and CSRO on a few of the static properties. Using the full width at half maximum of the radial distribution function of the atomic MEA structures,<sup>20</sup> it was found that increasing CSRO from RSS has the effect of reducing LD. The average LDs for the RSS, 950KCSRO, and 350KCSRO MEAs were estimated to be 5.401, 5.124, and 4.721 pm, respectively. In prior work, MS simulations were used to calculate an average intrinsic SFE for the A-atom, RSS, 950KCSRO, and 350KCSRO samples. Their values are, respectively,  $-25.26$ ,  $-14.97$ ,  $30.72$ , and  $82.6$  mJ/m<sup>2</sup>.<sup>20</sup> While odd, calculations of negative intrinsic SFE for this and other FCC MEAs are not unusual and have been reported previously.<sup>40,41</sup> It must be remembered that the A-atom and even the RSS MEA are unlike MEAs tested experimentally. Only the

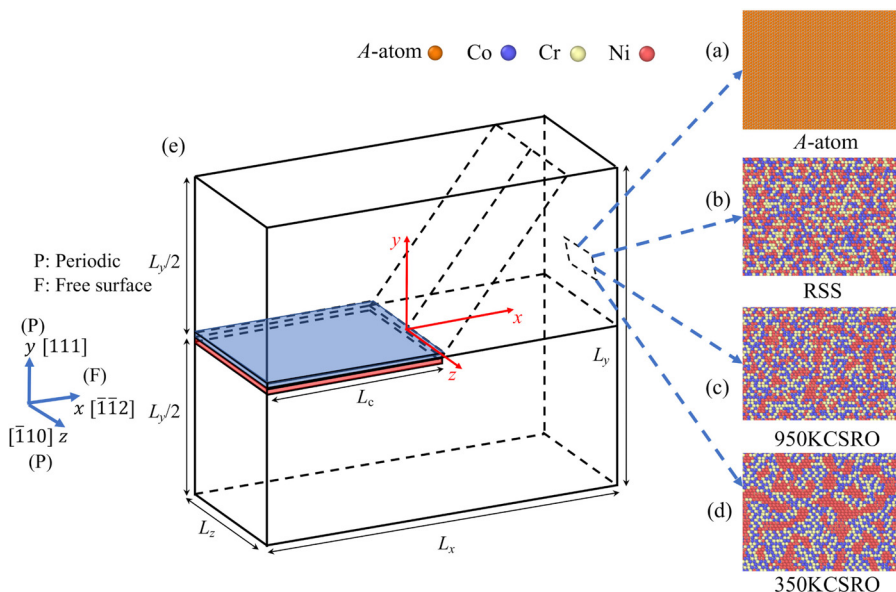


**FIG. 1.** Single crystal atomic configurations used in the simulations: (a) A-atom, (b) RSS, (c) 950KCSRO, and (d) 350KCSRO. (e) Schematic of the mode I crack geometry. The crack with a length of  $L_c = 10$  nm is created on the  $x$ - $z$  plane with its crack front along the  $z$  direction. The dislocation emitting from the crack tip glides on the  $(111)$  plane (the dashed plane) intersecting the  $x$ - $z$  plane.

MEAs with CSRO have been evidenced experimentally and these are the ones with positive intrinsic SFE values.

Once all models are built, a time step size of 1 fs is used in all remaining simulations. First, all materials are subject to dynamic relaxation with an NPT ensemble at 300 K with zero normal stresses along all three directions for 150 ps. After thermal relaxation, a through crack with a length of  $L_c = 10$  nm is created on the (111) plane at the middle position of  $L_y/2$  by blocking the interactions between two 1-nm-thick regions above and below the crack surface, denoted by the blue and red regions in Fig. 1(e), respectively. This method has also been utilized in many atomistic simulations of crack behavior<sup>42,43</sup> because it produces an ideally sharp crack. Conversely, if the cracks were formed by deleting a few layers of atoms, the crack would have been blunted.<sup>44</sup> The thickness of the simulation cell is sufficiently large (10 nm), making this a 3D cell. Then mode I loading is applied, by stretching the sample along the  $y$  axis at a constant strain rate of  $10^8$  s<sup>-1</sup>, resulting in a relative velocity of 6 m/s between the top and bottom layers of atoms. Periodic boundary conditions are imposed in the  $y$ - and  $z$ -directions, while the surfaces normal to the  $x$  axis are traction-free.<sup>45</sup> Zero normal stress along the  $z$  direction is maintained.

Figure 2 shows tensile force–displacement curves for the four crack-containing samples: A-atom, RSS, 950KCSRO, and 350KCSRO. After yielding, all materials show an initial strain hardening as the force is increased, which is a signature of stable inelastic deformation ahead of the crack tip. Eventually, the hardening response is terminated by rapid force release and softening of the curve, indicating the start of an unstable response. The area below the force–displacement curve up to the initiation of softening, multiplied by the cell volume, is 0.244, 0.117, 0.269, and 0.3 GPa, respectively, for the A-atom, RSS, 950KCSRO, and 350KCSRO samples. The RSS MEA is the least tough,

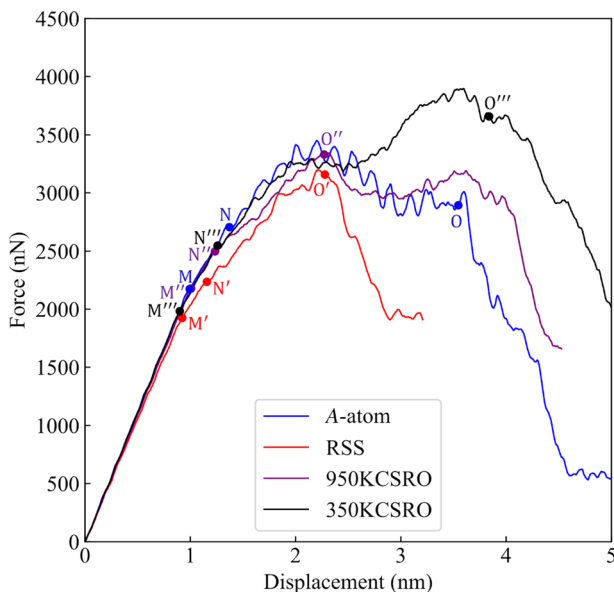


**FIG. 2.** Force–displacement curves of different samples under tension.  $M$ ,  $M'$ ,  $M''$ , and  $M'''$  correspond to the moments of the initial dislocation emission from the crack tip in the four samples, respectively. Similarly,  $N$ ,  $N'$ ,  $N''$ , and  $N'''$  are related to twin formation, while  $O$ ,  $O'$ ,  $O''$ , and  $O'''$  are the dislocation emission starting on a secondary slip system.

despite it possessing LD and chemical heterogeneity, suggesting that CSRO plays a more important role than LD in enhancing fracture toughness.

In the early period of loading, the responses of all four sample types are similar. However, at larger displacements, greater than that at which the A-atom and RSS samples have become unstable, the force in the two CSRO alloys continues to rise, suggesting different deformation events are at play. Of special note, the MEA with the larger degree of CSRO reaches the highest peak force and largest failure displacement among all samples.

We then probe the sequence of crack tip events underlying the force–displacement curves. Analysis in Fig. 3 finds that the first event to occur in all samples is a Shockley partial dislocation emitted ahead of the crack tip, before it propagates on the (11 $\bar{1}$ ) plane creating a stacking fault. The slip system is the same in all samples. In the A-atom metal, the atomic structure is distorted ahead of the crack tip, but to a lesser degree than the MEAs. The moments on the curves for the onset of dislocation nucleation are indicated by  $M$ ,  $M'$ ,  $M''$ , and  $M'''$  for A-atom sample, RSS, 950KCSRO, and 350KCSRO, respectively. The critical force for dislocation emission is the lowest in the RSS sample, while highest in the A-atom one. With the RSS MEA bearing the highest LD and the A-atom possessing none, we conclude that LD lowers the energy barrier for dislocation emission, in agreement with Zhu *et al.*<sup>31</sup> Relatedly, prior MD studies of crack-free single crystalline and nanocrystalline CoCrNi also found that LD lowered the stress to nucleate dislocations.<sup>20</sup> Another recent study in CoCrFeMnNi MPEA showed that the LD produces a heterogeneous stress field and those regions that experience higher stress are sites that promote dislocation formation.<sup>46</sup>

Through its effect on reducing LD, increasing CSRO above RSS can have an indirect effect on dislocation emission. However, the CSRO can also have a direct effect on the process of dislocation nucleation since the scale of the clustering is similar to the activation volume of dislocation formation. Figure 4 shows the atomic configurations at different displacements in the 350KCSRO CoCrNi. It is observed that the dislocation nucleation site corresponds to a CoCr cluster. Preferential dislocation emission from CoCr clusters at the crack-tip is also seen in the 950KCSRO sample, although the critical force for dislocation emission is higher than that for the 350KCSRO sample. The implication is that plastic deformation is promoted by higher levels of CSRO. The force for the first partial emission is the lowest in the RSS. The trends seen from the crack-tip are consistent with what has been learned from prior studies on dislocation nucleation on stressed single crystals and nanocrystalline samples of CoCrNi MEA with the same two degrees of CSRO.<sup>17,20,47</sup> They showed that CoCr regions in the single crystal were preferred nucleation sites and in the nanocrystalline material, dislocations first formed from the CoCr regions near the grain boundaries.

Following dislocation emission from the crack tip, the force and displacement rise as the dislocation glides away and a second partial is emitted on an adjacent plane parallel to the one where the first partial is emitted and glides in the same direction. After some amount of displacement, a nanotwin forms at the same site as dislocation nucleation and builds on the same glide plane in all samples, as marked by labels associated with  $N$  in Fig. 3. For the RSS MEA, the nanotwin forms at the lowest displacement and force, and nanotwinning reduces the hardening response and causes it to deviate from the response of other samples.



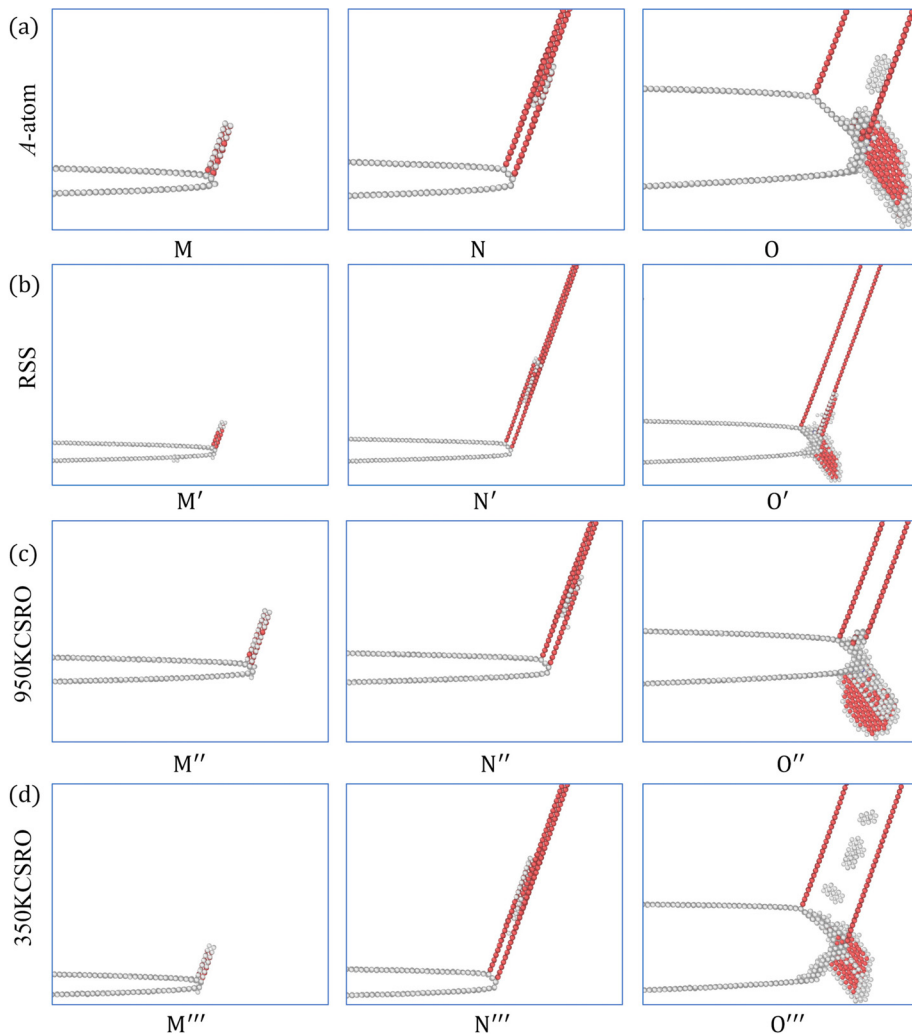


**FIG. 3.** Snapshots of dislocation emission, nanotwinning, and secondary slip system activation at the crack tip in different samples. The HCP atoms and those with unknown coordination structures are colored red and gray, respectively. Labels associated with M, N, and O are denoted on the force–displacement curves in Fig. 2.

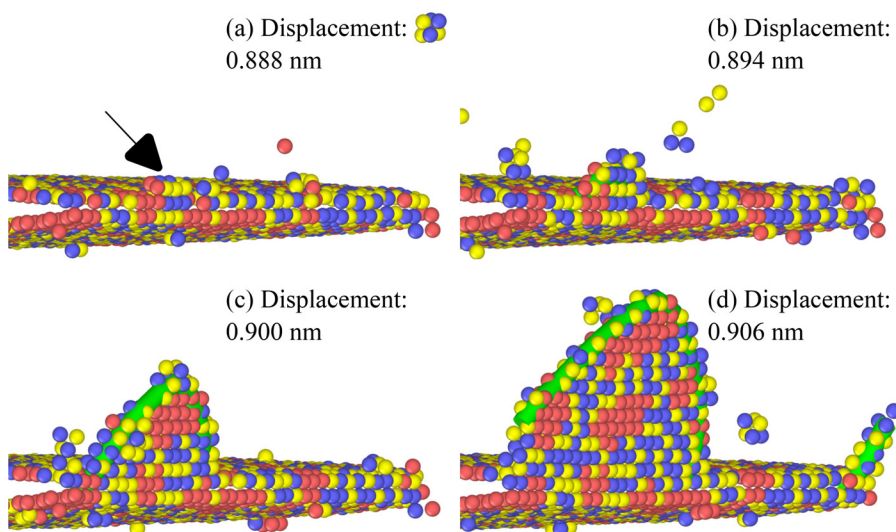


**FIG. 4.** Atomic configurations associated with dislocation nucleation at the crack tip in 350KCSRO CoCrNi MEA. The green curve indicates the partial dislocation. The atomic coloring follows that in Fig. 1, except that all FCC atoms have been visually removed. The CoCr cluster pointed to by an arrow in (a) is the site of the subsequent partial dislocation nucleation.

22 April 2024 16:10:21

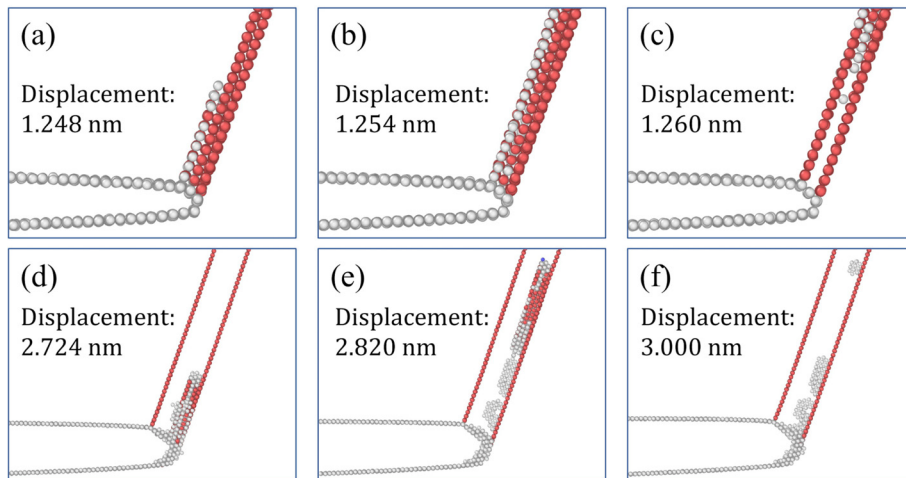


**FIG. 5.** Snapshots of the nucleation and development of nanotwins and the onset of amorphization at the crack tip in 350KCSRO CoCrNi MEA. The atomic coloring follows that in Fig. 3.

In all cases, nanotwinning causes the crack tip to become more blunted. As an example, Figs. 5(a)–5(c) show snapshots of the nanotwin nucleation process at the crack tip in the 350KCSRO CoCrNi, starting with the two-layer stacking fault. A second partial is emitted from the crack front in Fig. 5(a), then propagates on the two-layer stacking fault and along the same slip direction in Fig. 5(b). With a force increment, the three-layer fault transitions to a nanotwin, signified by the transition of the middle atomic layer from HCP to FCC [Fig. 5(c)]. This sequential glide process of Shockley partials to build a three-layer twin embryo is the same as the twinning process seen from grain boundaries<sup>48,49</sup> and interfaces<sup>50</sup> in pure FCC metals and alloys.

After nanotwin nucleation, the crack does not propagate significantly but rather increasing forces drive the nanotwin to thicken (Fig. 3). The twins grow by further emission of partials from the crack tip on the coherent twin boundary. Nanotwin growth is a toughening mechanism that occurs in all samples, even without chemical heterogeneity and/or CSRO. On the one hand, CoCrNi is known for easily producing wide stacking faults and stacking fault clusters and nanotwins.<sup>15</sup> On the other hand, nanotwinning at the crack tip occurs even in the A-atom metal. Accordingly, nanotwinning alone is not directly responsible for the good fracture toughness of this MEA.

In the RSS MEA, as the displacement increases further, a partial dislocation emits onto a secondary slip system, non-planar to the nanotwin as shown in Fig. 3(b). As the partial glides in the secondary slip system, the crack tip opens up further. Secondary slip occurs at the moment at point O in Fig. 2 and marks the onset of softening, leading to the reduced strength and lower toughness of the RSS sample compared to the CSRO samples. Similarly, in the A-atom sample, the activation of secondary slip also marks the onset of softening, but at greater displacement, marked as point O in Fig. 2. Accordingly, the nanotwin has the opportunity to grow thicker. The relatively early onset of secondary partial dislocation emission is favored over nanotwin growth in the RSS MEA because it has the lowest dislocation nucleation stress with the highest LD and the lowest intrinsic SFE. The A-atom's sample intrinsic SFE is similarly very low in this regard, favoring secondary partial slip emission and glide, albeit at greater displacements.

In Fig. 2, the two CSRO samples exhibit a second strain hardening, unlike the A-atom and RSS samples. The analysis finds that in both CSRO alloys, the second hardening response initiates with the

emission of a leading Shockley partial from the crack tip that glides within the nanotwin domain. The sequence of steps for the 350KCSRO MEA is shown in Figs. 5(d)–5(f). First, a stacking fault originates from the crack tip, and the leading partial glides away. As the force increases, the trailing partial emits and the perfect dislocation with a wide stacking fault glides further away from the crack front, leaving behind some amorphous debris [Figs. 5(e) and 5(f)]. Eventually, after these deformation events develop in the nanotwin, a partial dislocation on the secondary slip system emits into the crystal at moment O'' marked in Fig. 2, initiating rapid force release. Likewise, in the 950KCSRO MEA, the second rise is also attributed to the glide of leading partials within the nanotwin domain. However, in this lower CSRO MEA, the corresponding trailing partials do not emit. Instead, with a larger force, more leading partials emit on the secondary slip system, causing the crack tip to open up and initiating abrupt softening. Thus, plasticity within the nanotwin domain occurs but is not as extensive as in the 350KCSRO MEA.

In summary, using hybrid MD/MC simulations, we investigate the role of LD and CSRO on the deformation mechanisms ahead of a mode I crack in CoCrNi. The RSS MEA and two other MEAs exhibiting different degrees of CSRO are considered. An A-atom sample that is a chemically homogeneous counterpart with zero LD, but the same lattice constant and elastic properties, is also studied to assess the effects of both LD and CSRO. Simulations show that, in all four samples at the first stage of loading, partial dislocations are emitted from the crack tip, and with further increments in force, more partials are sequentially emitted on adjacent planes building a nanotwin. The only distinctive behavior occurs later at larger displacements, wherein the two CSRO MEAs manifest a second hardening response, while the RSS and A-atom samples have already become unstable. Our work suggests that in CoCrNi, CSRO plays a substantial role in its superior toughness.

W.J. and I.J.B. would like to acknowledge funding in part from the Office of Naval Research under Grant No. N00014-21-1-2536. Use was made of computational facilities purchased with funds from the National Science Foundation (No. CNS-1725797) and administered by the Center for Scientific Computing (CSC).

The CSC was supported by the California NanoSystems Institute and the Materials Research Science and Engineering Center (MRSEC; NSF DMR 2308708) at UC Santa Barbara.

## AUTHOR DECLARATIONS

### Conflict of Interest

The authors have no conflicts to disclose.

### Author Contributions

**Wu-Rong Jian:** Conceptualization (equal); Data curation (equal); Formal analysis (equal); Investigation (equal); Methodology (equal); Software (equal); Visualization (equal); Writing – original draft (equal). **Shuozhi Xu:** Validation (equal); Visualization (equal); Writing – review & editing (equal). **Dengke Chen:** Conceptualization (equal); Validation (equal). **Irene Beyerlein:** Funding acquisition (equal); Project administration (equal); Resources (equal); Supervision (equal); Writing – review & editing (equal).

### DATA AVAILABILITY

The data that support the findings of this study are available from the corresponding author upon reasonable request.

## REFERENCES

- S. Chen, W. Li, X. Xie, J. Brechtel, B. Chen, P. Li, G. Zhao, F. Yang, J. Qiao, and P. K. Liaw, “Nanoscale serration and creep characteristics of  $Al_{0.5}CoCrCuFeNi$  high-entropy alloys,” *J. Alloys Compd.* **752**, 464–475 (2018).
- Z. Li, S. Zhao, R. O. Ritchie, and M. A. Meyers, “Mechanical properties of high-entropy alloys with emphasis on face-centered cubic alloys,” *Prog. Mater. Sci.* **102**, 296–345 (2019).
- B. Cantor, “Multicomponent and high entropy alloys,” *Entropy* **16**, 4749–4768 (2014).
- Y. Ye, Q. Wang, J. Lu, C. Liu, and Y. Yang, “High-entropy alloy: Challenges and prospects,” *Mater. Today* **19**, 349–362 (2016).
- E. Pickering and N. Jones, “High-entropy alloys: A critical assessment of their founding principles and future prospects,” *Int. Mater. Rev.* **61**, 183–202 (2016).
- E. George, W. Curtin, and C. C. Tasan, “High entropy alloys: A focused review of mechanical properties and deformation mechanisms,” *Acta Mater.* **188**, 435–474 (2019).
- B. Gludovatz, A. Hohenwarter, K. V. Thurston, H. Bei, Z. Wu, E. P. George, and R. O. Ritchie, “Exceptional damage-tolerance of a medium-entropy alloy CrCoNi at cryogenic temperatures,” *Nat. Commun.* **7**, 10602 (2016).
- Z. Zhang, H. Sheng, Z. Wang, B. Gludovatz, Z. Zhang, E. P. George, Q. Yu, S. X. Mao, and R. O. Ritchie, “Dislocation mechanisms and 3D twin architectures generate exceptional strength-ductility-toughness combination in CrCoNi medium-entropy alloy,” *Nat. Commun.* **8**, 14390 (2017).
- D. Liu, Q. Yu, S. Kabra, M. Jiang, P. Forna-Kreutzer, R. Zhang, M. Payne, F. Walsh, B. Gludovatz, M. Asta *et al.*, “Exceptional fracture toughness of CrCoNi-based medium- and high-entropy alloys at 20 kelvin,” *Science* **378**, 978–983 (2022).
- H. S. Oh, D. Ma, G. P. Leyson, B. Grabowski, E. S. Park, F. Körmann, and D. Raabe, “Lattice distortions in the FeCoNiCrMn high entropy alloy studied by theory and experiment,” *Entropy* **18**, 321 (2016).
- Y. Zhao, Z. Lei, Z. Lu, J. Huang, and T. Nieh, “A simplified model connecting lattice distortion with friction stress of Nb-based equiatomic high-entropy alloys,” *Mater. Res. Lett.* **7**, 340–346 (2019).
- R. Zhang, S. Zhao, J. Ding, Y. Chong, T. Jia, C. Ophus, M. Asta, R. O. Ritchie, and A. M. Minor, “Short-range order and its impact on the CrCoNi medium-entropy alloy,” *Nature* **581**, 283–287 (2020).
- X. Chen, Q. Wang, Z. Cheng, M. Zhu, H. Zhou, P. Jiang, L. Zhou, Q. Xue, F. Yuan, J. Zhu, W. Xiaolei, and E. Ma, “Direct observation of chemical short-range order in a medium-entropy alloy,” *Nature* **592**, 712–716 (2021).
- D. L. Foley, A. K. Barnett, Y. Rakita, A. Perez, P. P. Das, S. Nicolopoulos, D. E. Spearot, I. J. Beyerlein, M. L. Falk, and M. L. Taheri, “Diffuse electron scattering reveals kinetic frustration as origin of order in CoCrNi medium entropy alloy,” *Acta Mater.* **268**, 119753 (2024).
- Q.-J. Li, H. Sheng, and E. Ma, “Strengthening in multi-principal element alloys with local-chemical-order roughened dislocation pathways,” *Nat. Commun.* **10**, 3563 (2019).
- S. Mubassira, W.-R. Jian, and S. Xu, “Effects of chemical short-range order and temperature on basic structure parameters and stacking fault energies in multi-principal element alloys,” *Modelling* **5**, 352–366 (2024).
- A. Gupta, W.-R. Jian, S. Xu, I. J. Beyerlein, and G. J. Tucker, “On the deformation behavior of CoCrNi medium entropy alloys: Unraveling mechanistic competition,” *Int. J. Plast.* **159**, 103442 (2022).
- G. Huang, X. Zhang, R. Zhang, W.-R. Jian, X. Zou, K. Wang, Z. Xie, and X. Yao, “The shear softening and dislocation glide competition due to the shear-induced short-range order degeneration in CoCrNi medium-entropy alloy,” *J. Mater. Sci. Technol.* **192**, 108–122 (2024).
- D. Hua, Q. Xia, W. Wang, Q. Zhou, S. Li, D. Qian, J. Shi, and H. Wang, “Atomistic insights into the deformation mechanism of a CoCrNi medium entropy alloy under nanoindentation,” *Int. J. Plast.* **142**, 102997 (2021).
- W.-R. Jian, Z. Xie, S. Xu, Y. Su, X. Yao, and I. J. Beyerlein, “Effects of lattice distortion and chemical short-range order on the mechanisms of deformation in medium entropy alloy CoCrNi,” *Acta Mater.* **199**, 352–369 (2020).
- D. Hua, X. Liu, W. Wang, Q. Zhou, Q. Xia, S. Li, J. Shi, and H. Wang, “Formation mechanism of hierarchical twins in the CoCrNi medium entropy alloy,” *J. Mater. Sci. Technol.* **140**, 19–32 (2023).
- W.-R. Jian, L. Wang, W. Bi, S. Xu, and I. J. Beyerlein, “Role of local chemical fluctuations in the melting of medium entropy alloy CoCrNi,” *Appl. Phys. Lett.* **119**, 121904 (2021).
- Z. Xie, W.-R. Jian, S. Xu, I. J. Beyerlein, X. Zhang, Z. Wang, and X. Yao, “Role of local chemical fluctuations in the shock dynamics of medium entropy alloy CoCrNi,” *Acta Mater.* **221**, 117380 (2021).
- L. Zhu, X. Zhang, W.-R. Jian, Z. Xie, and X. Yao, “Plastic deformation mechanism and defect patterning under nanoindentation in medium entropy alloy CoCrNi,” *J. Alloys Compd.* **968**, 171734 (2023).
- G. Huang, X. Zhang, Z. Xie, W.-R. Jian, R. Zhang, and X. Yao, “Effects of lattice distortion and chemical short-range order on creep behavior of medium-entropy alloy CoCrNi,” *Mech. Mater.* **177**, 104549 (2023).
- Z. Xie, W.-R. Jian, S. Xu, I. J. Beyerlein, X. Zhang, X. Yao, and R. Zhang, “Phase transition in medium entropy alloy cocrni under quasi-isentropic compression,” *Int. J. Plast.* **157**, 103389 (2022).
- W.-R. Jian, Z. Xie, S. Xu, X. Yao, and I. J. Beyerlein, “Shock-induced amorphization in medium entropy alloy CoCrNi,” *Scr. Mater.* **209**, 114379 (2022).
- H. Wang, D. Chen, X. An, Y. Zhang, S. Sun, Y. Tian, Z. Zhang, A. Wang, J. Liu, M. Song *et al.*, “Deformation-induced crystalline-to-amorphous phase transformation in a CrMnFeCoNi high-entropy alloy,” *Sci. Adv.* **7**, eabe3105 (2021).
- J. Li, H. Chen, Q. He, Q. Fang, B. Liu, C. Jiang, Y. Liu, Y. Yang, and P. K. Liaw, “Unveiling the atomic-scale origins of high damage tolerance of single-crystal high entropy alloys,” *Phys. Rev. Mater.* **4**, 103612 (2020).
- D. Farkas, “The role of compositional complexity in the increased fracture resistance of high entropy alloys: Multi-scale atomistic simulations,” *Comput. Mater. Sci.* **235**, 112758 (2024).
- X. Zhu, F. Cao, L. Dai, and Y. Chen, “Effects of chemical short-range order and lattice distortion on crack-tip behavior of medium-entropy alloy by atomistic simulations,” *Metals* **14**, 226 (2024).
- A. P. Thompson, H. M. Aktulga, R. Berger, D. S. Bolintineanu, W. M. Brown, P. S. Crozier, P. J. in ’t Veld, A. Kohlmeyer, S. G. Moore, T. D. Nguyen, R. Shan, M. J. Stevens, J. Tranchida, C. Trott, and S. J. Plimpton, “LAMMPS—A flexible simulation tool for particle-based materials modeling at the atomic, meso, and continuum scales,” *Comput. Phys. Commun.* **271**, 108171 (2022).
- F.-H. Cao, Y.-J. Wang, and L.-H. Dai, “Novel atomic-scale mechanism of incipient plasticity in a chemically complex CrCoNi medium-entropy alloy associated with inhomogeneity in local chemical environment,” *Acta Mater.* **194**, 283–294 (2020).

- <sup>34</sup>I. A. Alhafez, C. J. Ruestes, S. Zhao, A. M. Minor, and H. M. Urbassek, "Dislocation structures below a nano-indent of the CoCrNi medium-entropy alloy," *Mater. Lett.* **283**, 128821 (2020).
- <sup>35</sup>C. Varvenne, A. Luque, W. G. Nöhring, and W. A. Curtin, "Average-atom interatomic potential for random alloys," *Phys. Rev. B* **93**, 104201 (2016).
- <sup>36</sup>W.-R. Jian, "CoCrNi A-atom potential," [https://github.com/wrj2018/Acta\\_2020](https://github.com/wrj2018/Acta_2020). Accessed: April 12, 2024.
- <sup>37</sup>P. M. Larsen, S. Schmidt, and J. Schiøtz, "Robust structural identification via polyhedral template matching," *Modell. Simul. Mater. Sci. Eng.* **24**, 055007 (2016).
- <sup>38</sup>A. Stukowski, "Visualization and analysis of atomistic simulation data with OVITO—The open visualization tool," *Modell. Simul. Mater. Sci. Eng.* **18**, 015012 (2009).
- <sup>39</sup>S. Xu, E. Hwang, W.-R. Jian, Y. Su, and I. J. Beyerlein, "Atomistic calculations of the generalized stacking fault energies in two refractory multi-principal element alloys," *Intermetallics* **124**, 106844 (2020).
- <sup>40</sup>Y. H. Zhang, Y. Zhuang, A. Hu, J. J. Kai, and C. T. Liu, "The origin of negative stacking fault energies and nano-twin formation in face-centered cubic high entropy alloys," *Scr. Mater.* **130**, 96–99 (2017).
- <sup>41</sup>D. You, O. K. Celebi, A. S. K. Mohammed, and H. Sehitoglu, "Negative stacking fault energy in FCC materials-Its implications," *Int. J. Plast.* **170**, 103770 (2023).
- <sup>42</sup>X. R. Zhuo, J. H. Kim, and H. G. Beom, "Atomistic investigation of crack growth resistance in a single-crystal Al-nanoplate," *J. Mater. Res.* **31**, 1185 (2016).
- <sup>43</sup>P. Andric and W. Curtin, "New theory for crack-tip twinning in fcc metals," *J. Mech. Phys. Solids* **113**, 144–161 (2018).
- <sup>44</sup>P. Andric and W. Curtin, "New theory for Mode I crack-tip dislocation emission," *J. Mech. Phys. Solids* **106**, 315–337 (2017).
- <sup>45</sup>S. Xu, L. Xiong, Q. Deng, and D. L. McDowell, "Mesh refinement schemes for the concurrent atomistic-continuum method," *Int. J. Solids Struct.* **90**, 144–152 (2016).
- <sup>46</sup>J. Li, Y. Chen, Q. He, X. Xu, H. Wang, C. Jiang, B. Liu, Q. Fang, Y. Liu, Y. Yang, P. K. Liaw, and C. T. Liu, "Heterogeneous lattice strain strengthening in severely distorted crystalline solids," *Proc. Natl. Acad. Sci. U. S. A.* **119**, e2200607119 (2022).
- <sup>47</sup>N. Rasooli, W. Chen, and M. Daly, "Deformation mechanisms in high entropy alloys: A minireview of short-range order effects," *Nanoscale* **16**, 1650–1663 (2024).
- <sup>48</sup>X. Zhao, C. Lu, A. K. Tieu, L. Zhan, M. Huang, L. Su, L. Pei, and L. Zhang, "Deformation twinning and dislocation processes in nanotwinned copper by molecular dynamics simulations," *Comput. Mater. Sci.* **142**, 59–71 (2018).
- <sup>49</sup>T. L. Dora, S. K. Singh, R. R. Mishra, E. R. Homer, S. Ogata, and A. Verma, "Deformation and boundary motion analysis of a faceted twin grain boundary," *Int. J. Mech. Sci.* **269**, 109044 (2024).
- <sup>50</sup>Y. Zheng, Q. Li, J. Zhang, H. Ye, H. Zhang, and L. Shen, "Hetero interface and twin boundary mediated strengthening in nano-twinned Cu//Ag multilayered materials," *Nanotechnology* **28**, 415705 (2017).